Transitions of turbulence in plasma density limits[a)]

X. Q. Xu,[b)] W. M. Nevins, T. D. Rognlien, R. H. Bulmer, M. Greenwald,[c)] A. Mahdavi,[d)] L. D. Pearlstein, and P. Snyder[d)]
Lawrence Livermore National Laboratory, Livermore, California 94551

(Received 14 November 2002; accepted 14 February 2003)

A series of BOUT [X. Q. Xu *et al.*, Phys. Plasmas **7**, 1951 (2000)] simulations is conducted to investigate the physical processes which limit the density in tokamak plasmas. Simulations of turbulence in tokamak boundary plasmas are presented which show that turbulent fluctuation levels and transport increase with collisionality. At high edge density, the perpendicular turbulent transport dominates the parallel classical transport, leading to substantially reduced contact with divertor plates and the destruction of the edge shear layer, and the region of high transport then extends inside the last closed flux surface. As the density increases these simulations show resistive X-point mode→resistive ballooning modes. The simulations also show that it is easier to reach the density limit as the density increases while holding pressure constant than holding temperature constant. A set of 2D transport simulations with increasingly large radial outboard transport, as indicated by BOUT for increasing density, shows that such transport can lead to an X-point multifaced asymmetric radiation from the edge when impurity radiation is included, which is a common symptom of density-limit related disruptions. BOUT further demonstrates that the local transport scaling with the current is similar to the global low-confinement-mode (L-mode) transport model ($\tau_E \propto I_p$) (by fixing q profiles). This current scaling appears on a plot of discharge current versus density as abruptly large radial transport once the Greenwald density is approached or exceeded. All of these results indicate that rapid edge cooling due to large radial transport is a key for the physics of the tokamak density limit. © *2003 American Institute of Physics.* [DOI: 10.1063/1.1566032]

I. INTRODUCTION

Scaling of experimental data from many tokamaks with gas fueling has indicated the presence of a maximum electron density above which the frequency of disruptive terminations increases rapidly. Disruptive termination at the density limit is frequently correlated with growth of magnetohydrodynamic (MHD) modes with low toroidal and poloidal mode numbers. By examining data both from ohmically heated and neutral beam-heated tokamak discharges, Greenwald *et al.* concluded[1] that this disruptive limit was given by the relation $\overline{n_e} > n_G = I_p/\pi a^2$, where $\overline{n_e}$ is the line-averaged electron density in 10^{20} m^{-3}, n_G is in 10^{20} m^{-3}, I_p is the plasma current in mega-Ampères (MA), and a is the minor radius in meters. Even though this empirical scaling is obtained for elliptical tokamak plasmas; the simple law works for a wide variety of machine sizes and configurations. Thus the Greenwald density n_G becomes a common figure of merit for high-density operation. The global scaling, however, does miss important local effects, in particular, the role of the density profile. Discharges with good confinement are achieved at densities above the empirical limit by pellet fueling with significant central density peaking[2,3] and by gas fueling with only moderate density peaking[4] in DIII-D H-mode plasmas. The comprehensive experimental observations and theoretical developments for density limit in toroidal plasma have been recently surveyed in an excellent review paper by Greenwald.[5]

Obtaining high energy confinement at high density is important since the fusion power increases with density as $P_{\mathrm{FUS}} \propto n^2 \langle \sigma v \rangle$, where n is the ion density and $\langle \sigma v \rangle$ is the fusion reaction rate. However, the Greenwald empirical scaling shows that the maximum attainable plasma density is limited by the plasma current, which is in turn limited by MHD kink instabilities. While density limits have been observed for several decades, there is no widely accepted first-principles theory available. For the tokamak, there is a generally accepted picture for the density limit which involves edge cooling, current profile shrinkage followed by the loss of MHD equilibrium.[6] What leads to edge cooling and the collapse of current profile? A number models have been proposed to explain an increase in transport at high densities and its relation to the density limit. Theoretical considerations of the thermal stability of a current carrying plasma column and experimental observations which associated disruptive plasmas with high levels of impurities led investigators to propose these mechanisms for the density limit. Several scenarios have been considered. In the first, radiation from high Z impurities in the plasma core leads to cooling across the entire profile and to neoclassical tearing mode caused by density peaking.[4] In the second scenario, impurity radiation leads to a thermal condensation in the plasma edge by competing effectively with heat transport. The appearance of these condensations, or multifaced asymmetric radiation from the edge (MARFE), has been shown to scale in the

[a)]Paper UI2 3, Bull. Am. Phys. Soc. **47**, 324 (2002).
[b)]Invited speaker.
[c)]MIT-Plasma Science & Fusion Center, 175 Albany Street, Cambridge, MA 02139.
[d)]General Atomics, San Diego, CA 92186.

same manner as the density limit.[2,7] While the radiation models have had some success in explaining experimental results, they have shortcomings which suggest that they are incomplete at best. The various models seek to identify the density limit with $P_{\mathrm{rad}}/P_{\mathrm{in}} \sim 1.0$, MARFE formation, poloidal detachment, or divertor detachment. These phenomena all exhibit density threshold behavior, but experimental thresholds can range as low as a quarter of the ultimate density limit. Moreover, these models generally predict strong sensitivity to power input and impurity content and often to details of divertor or limiter geometry. They depend on models for heat and particle transport which do not necessarily match experimental observations. The overarching question is whether radiation related phenomena are a cause of the density limit or a common symptom of some other physics which drives edge cooling—namely density-dependent transport. In other words, is there a maximum density independent of atomic processes? Does edge transport increase strongly as the density is raised above a critical value and is this increase the fundamental driver for the limit? Three-dimensional nonlinear two-fluid simulations in flux tube geometry have found a region of exceptionally high transport in low-temperature and high-density regimes,[8] which are typical near the density limit. The role of divertor or limiter sheath physics on turbulence on open field lines has been recently addressed.[9] In these studies, large coherent structures (''blobs'') undergo ∇B polarization and drift rapidly across the SOL under the influence of the resultant $E \times B$ drift.

In this article, 3D BOUT[10] turbulence simulations and 2D UEDGE[11] transport simulations are conducted to investigate the physical processes which limit density in tokamak plasmas. Simulations of turbulence in tokamak boundary plasmas are presented which show that turbulent fluctuation levels and transport increase with collisionality. At high density, the perpendicular turbulent transport dominates the parallel classical transport in the scrape-off layer (SOL), leading to a reduced impact of the divertor and to the destruction of the edge shear layer; the region of high transport then extends inside the last closed flux surface (LCFS). As the density increases these simulations show resistive X-point mode→resistive ballooning mode→detachment from divertor. Thus, our density limit scenario is as follows: The large perpendicular transport peaked on the outside of torus changes the dominant loss channel from divertor to the main chamber, which is accompanied by a shift of the peak plasma density from the divertor plate region to the region near the X-point. The higher density and lower temperature near the X-point then lead to a MARFE with strong radiation losses. The enhanced losses cause the plasma column to shrink and discharge to be disrupted due to long wavelength magneto-hydrodynamic (MHD) modes. Here we only model the initial change in the edge turbulence and some aspects of MARFE formation.

The rest of the article is organized as follows: In Sec. II the general turbulence characteristics of high-density simulation are described. In this section, we discuss the transition of turbulence characteristics near the plasma density limit. In Sec. III we consider the roles of the divertor plasma and impurity radiation in high-density simulations. The turbulence transport and its relation to density limit scaling with current is presented in Sec. IV. A summary and discussion are given in Sec. V.

II. CHARACTERISTICS OF HIGH DENSITY SIMULATIONS

BOUT models boundary-plasma turbulence in a realistic divertor geometry using modified Braginskii equations[12] in 3D for plasma vorticity ϖ, density (n_i), electron and ion temperatures (T_e, T_i), and parallel momenta. The electrostatic potential ϕ and parallel magnetic potential $A_{\|}$ are also calculated. The dynamical equations, boundary conditions, and numerical scheme are discussed in Refs. 10 and 13. All results reported in this article were obtained by BOUT and UEDGE simulations for a deuterium tokamak plasma with a diverted, lower single-null magnetic equilibrium. Only low-confinement-mode (L-mode) discharges are investigated in this article.

A. General turbulence characteristics

To simulate boundary plasma turbulence and validate with the corresponding experiments, the BOUT code uses realistic X-point magnetic and plasma profiles. The background magnetic field structure is obtained from a MHD equilibrium code (usually EFIT[14]) for a typical shot. The plasma profiles are obtained by taking density and temperature as analytic fits (modified tanh) to Thomson scattering data (Fig. 1). For the scaling studies with plasma current, the background magnetic field structure is obtained from another MHD equilibrium code, Corsica.[15] For typical DIII-D boundary plasma profiles in L-mode, the midplane values on the magnetic separatrix are $T_e = 60$ eV, $T_i = 240$ eV, and $n_i = 6.5 \times 10^{18}/\mathrm{m}^3$. From the given magnetic geometry and plasma profiles corresponding to a specific experimental device and discharge, the simulation is initialized with a set of small random fluctuations. The fastest growing modes dominate the initial phase of the calculation, in which the fluctuations grow at an approximately exponential rate. After this initial linear phase, the density and electrostatic potential fluctuations evolve to a saturated state with many modes, as shown in Fig. 2. The background density and temperature profiles are held constant during the turbulence evolution. However, the electric potential, parallel current and ion velocity are self-consistently evolved with turbulence dynamics. At $t \sim 43\ \mu$s, the unstable modes inside the separatrix enter into a nonlinear phase. After a period of adjustment, the turbulence-generated electric potential reaches a steady state. From the saturated steady state, turbulence statistical properties can be extracted from the BOUT simulations by using the correlation function analysis and validated with the various fluctuation measurements.[16–19] From the density contour plot (not shown) we observe the following as the density increases: (1) Large-scale, transient, and coherent structures convect in the ion poloidal diamagnetic velocity direction at ~1 km/s at low density and reverse to electron diamagnetic direction at high density at ~10 km/s outside the separatrix. (2) The fluctuation levels and the radial correlation length

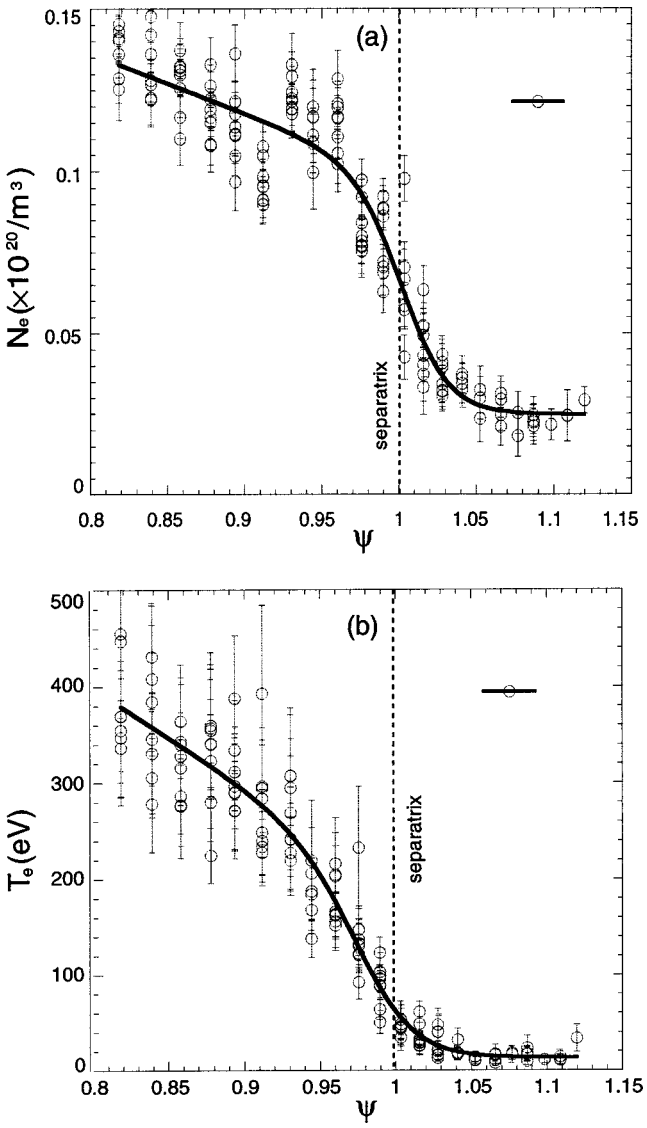

FIG. 1. Typical pedestal density and temperature profiles. DIII-D shot 107822 at time = 2900 ms. Figures courtesy of G. D. Porter at Lawrence Livermore National Laboratory.

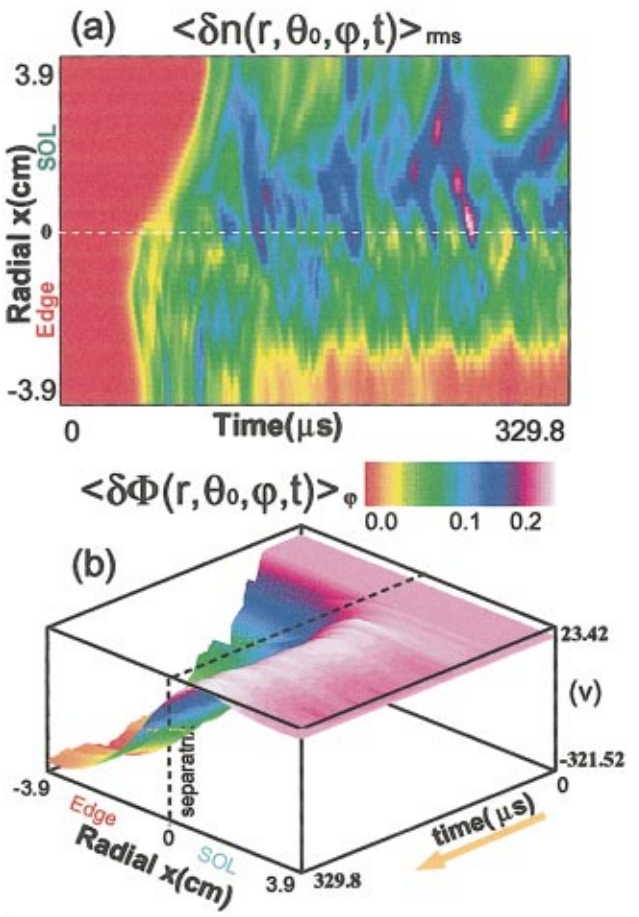

FIG. 2. (Color) (a) The time history of the root-mean-squared (rms) amplitude of fluctuating density at the outer midplane. (b) The flux surface averaged electric potential at the outside midplane. The density fluctuation scale in (a) is 25%.

increases, as indicated by the estimated perpendicular scale length, L_0, given by the resistive ballooning mode.[20] However, at low density, the BOUT radial correlation length is longer than that from the estimates, while at high density they agree inside the last closed flux surface.

B. Transition of turbulence characteristics near the plasma density limit

Recent studies of resistive ballooning modes in the boundary plasma of diverted tokamaks have been performed within the framework of a collisional fluid model.[10,21,22] It is shown that the large magnetic shear and small poloidal B-field in the X-point region act to increase the local perpendicular wavenumber, and hence the importance of the resistivity, near the X-point. This effect can be viewed as a consequence of the fanning of the flux tubes in the X-point region, and it has no simple analog in circular flux geometry where the magnetic shear, $\hat{s}$, is constant on a flux surface. As a result of the locally enhanced resistive effects, the mode can line-bend across the X-point, avoiding the good curvature region on the inside of the torus. This ''disconnection'' of the eigenmodes profoundly influences the unstable spectrum. A new class of modes called resistive X-point (RX) modes exploits this synergism between resistivity and the X-point geometry, giving rise to robust growth rates at moderate-to-low mode numbers for which resistive effects would otherwise be negligible. BOUT simulations indicate that although the radial and perpendicular mode structures evolve from linear to nonlinear phase due to nonlinear mode-coupling processes, the parallel mode structure stays the similar throughout the simulations.

To address issues related to density-dependent transport, we can step back from real experiments and examine the general behavior of the turbulence in the parameter space of edge density and temperature. Starting from a particular discharge which corresponds to a DIII-D L-mode experiment as a base case, two numerical experiments have been performed: (1) increasing density while holding pressure constant and (2) increasing density while holding temperature constant. These two cases separate the pressure driven instabilities from density-dependent instabilities. In the first case, the magnetic equilibrium is kept the same. If there is no edge

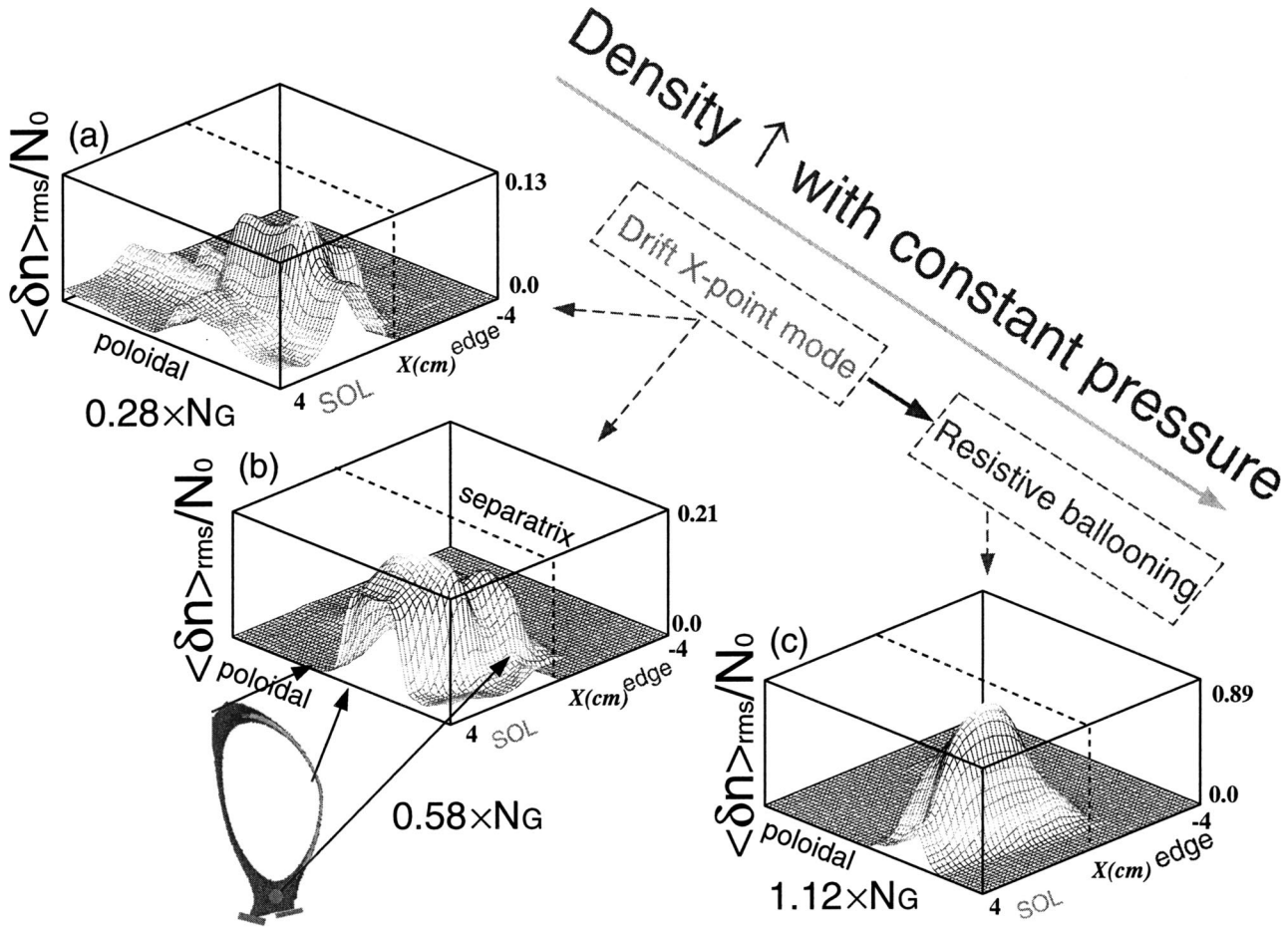

FIG. 3. The rms levels of the radial-poloidal profiles of fluctuation density calculated from BOUT simulation. As the Greenwald density is approached or exceeded, the SOL density fluctuation increases and peaked around the outer midplane. Here $N_0 = 1.2 \times 10^{19}/\mathrm{m}^3$.

localized mode (ELM) for the base case, there is also no ELM for the density scans due to the absence of current drive and constant pressure profiles for the scans. In the second case, one can take from the experimental observations the typical separatrix temperature $T_e \simeq 50$ eV, and far SOL temperature $T_e \simeq 10$ eV. However, the change of magnetic equilibrium is ignored in the simulations.

The corresponding root-mean-squared (rms) radial-poloidal mode structures are shown in Fig. 3 for the first case with three different background densities: (a) $\overline{n_e} = 0.28 n_G$, (b) $\overline{n_e} = 0.56 n_G$, and (c) $\overline{n_e} = 1.12 n_G$. Here $\overline{n_e}$ is the line-averaged density in $10^{20}\ \mathrm{m}^{-3}$, $n_G = I_p/\pi a^2$ in $10^{20}\ \mathrm{m}^{-3}$. For the base case (a) which corresponds to a DIII-D L-mode experiment, $I_p = 0.974$ MA, $a = 0.59$ m and $\overline{n_e} = 0.25 \times 10^{20}\ \mathrm{m}^{-3}$. The typical resistive X-point mode discussed above appears at the upper left corner of the plot as a base case. In this regime, the X-point effects are the most dramatic. The eigenfunction illustrates that the resistivity is dominant near the X-points, allowing the mode to decrease rapidly away from this region. In this particular case, the mode survives past the lower X-point and does weakly sample the outer divertor plasma. As density increases, moving diagonally down from the upper left corner of the plot, the rms fluctuation levels increase dramatically, and the modes are poloidally peaked around the outer midplane. For pressure conservation, as density increases while temperature decreases, one enters the strong resistive ballooning regime in lower right corner of the plot. In this case, ballooning of the eigenfunction at the outboard midplane reduces the importance of X-point effects, and it becomes classical resistive MHD mode. These results clearly demonstrate the transition from resistive X-point mode to resistive ballooning mode as the density approaches and exceeds the Greenwald density. A similar trend of the mode transition in the parameter space n_e and T_e has also been found in the linear eigenmode calculation.[22]

For case (2) where we increase density by a factor of 10 while holding temperature constant, we find that density fluctuation levels only increase by 50%. In contrast for case (1) in Fig. 4(a) the turbulence fluctuation levels increase by 500%, when the density increases by a factor of 4. This difference between the two cases is due to the strong temperature dependence in the collisionality ($\nu_{ei} \propto n/T_e^{3/2} \propto n^{5/2}/P_e^{3/2}$) and the resulting electron parallel conductivity ($\kappa_{\|e} \propto T_e^{5/2}$).

Particle transport perpendicular to the magnetic field, Γ_r, results from correlated fluctuations of the plasma drift velocity $\tilde{v}_E$ and density $\tilde{n}$, and can be calculated from $\Gamma_r = \langle \tilde{v}_E \tilde{n} \rangle$. A large particle flux is found near the X-point re-

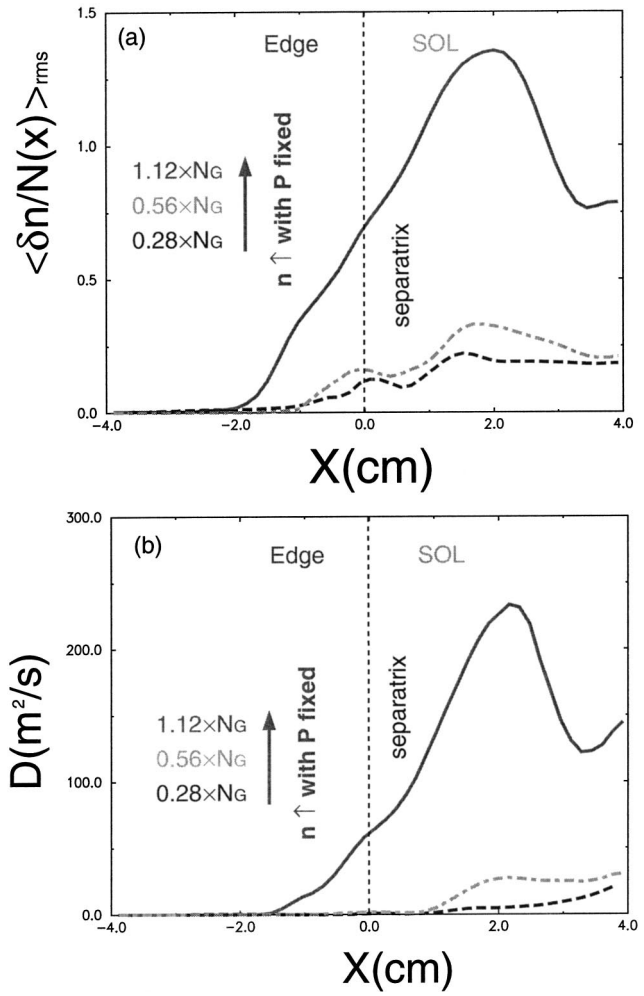

FIG. 4. Profiles of density fluctuation levels (a) and diffusion coefficients (b) calculated from BOUT simulation. As the Greenwald density is approached or exceeded, the SOL diffusivity increases and the region of high fluctuation levels and high diffusivity extend inward across the last closed flux surface. The solid curve for $n=1.12N_G$, dot–dashed curve for $n=0.56N_G$, and dashed curve for $n=0.28N_G$.

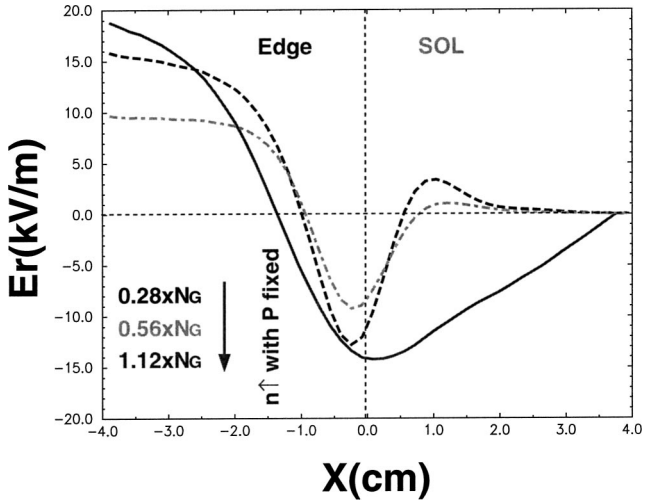

FIG. 5. Profiles of electric field calculated from BOUT simulation. As the Greenwald density is approached or exceeded, the edge E_r shear layer is destroyed. The solid curve for $n=1.12N_G$, dot–dashed curve for $n=0.56N_G$, and dashed curve for $n=0.28N_G$.

gion due to large $\tilde{v}_E$ there from large $k_\perp$ at low density. However, as the density increases, the particle flux is also peaked around the outer midplane (not shown). This is another evidence to show the mode transition from the resistive X-point mode to resistive ballooning mode as the density approaches and exceeds the Greenwald density.

Large increases in the effective diffusivity, $D_{\text{eff}}=-\Gamma_r/\nabla n$, are illustrated in Fig. 4(b) as the density limit is approached while the edge temperature and gradient drop precipitously. It also shows that as the density is increased, the strong E_r shear layer is destroyed (Fig. 5) and the region of high diffusivity extends inward. The negative E_r inside the separatrix is generated by the Reynolds stress, and positive E_r in the far SOL is dominated by the sheath physics due to parallel particle loss. Near the separatrix in the SOL, the two mechanisms compete. As density increases and temperature decreases, the fluctuation levels and the Reynolds stress drive increases while sheath potential decreases, so that the negative E_r extends outward. Eventually the Reynolds stress drive dominates over sheath drive in the SOL, and the strong E_r shear layer is destroyed as the density approaches or exceeds the Greenwald density. Figure 4(b) also shows that for the given magnetic equilibrium, as the density increases while temperature decreases, transport increases but manifests itself in nearly discontinuous behavior from $\overline{n}=0.56N_G$ to $\overline{n}=1.12N_G$. The implication is that a catastrophic boundary is crossed. Similar experimental results has been obtained on the Texas Experimental Tokamak (TEXT)[23] and Alcator C-mod.[24] On TEXT, the change in transport was correlated with a significant increase in low-frequency fluctuations with moderately high wave numbers, $k_\theta \sim 12\ \text{cm}^{-1}$ corresponding to $k_\theta \rho_s \sim 0.3-0.9$, where ρ_s is the ion gyroradius. Spatial resolution in these experiments was not sufficient to localize the source of the fluctuations. Data from a fast reciprocating probe showed a strong increase in fluctuations in the far SOL on DIII-D.[25] On ASDEX, a clear increase in correlation time and length were seen at higher densities.[26] An increase in turbulence driven flux with density was seen on the Joint European Torus (JET).[27] On C-Mod, measurements with a fast scanning electrostatic probe found two distinguishable regions in the SOL.[24] Near the separatrix, density and temperature profiles were steep, with gradient lengths of the order of 5 mm or shorter. The fluctuations in this region were of moderate amplitude, with autocorrelation times on the order of 1 μs. Using a high-resolution Lyman array to determine the ionization source, the particle transport could be calculated and convective losses estimated. The effective diffusivity $D_{\text{eff}}=-\Gamma_r/\nabla n$ was found to scale with the parallel collisionality as $(L_\parallel/\lambda_{ei})^{1.7}$, where Γ_r is the integrated particle source and λ_{ei} is the mean free path for electron-ion collisions. Flows down the open field lines to the divertor were found to be an unimportant component of the particle balance. Beyond this region, in the far SOL, profiles were much flatter and fluctuations were large and intermittent. The autocorrelation time for fluctuations in this region was of the order of 20–40 μs. The far SOL region had very large cross-field transport, well

in excess of parallel losses for both particles and energy. As the density was raised, the breakpoint between the two regions move inward toward the separatrix, which is consistent with Fig. 4(b).

III. ROLES OF DIVERTOR PLASMA AND IMPURITY RADIATION

The simplest models for MARFE formation involve only radiation, parallel conduction, and a heat source from perpendicular transport. A thermal collapse or condensation can occur at temperatures where the cooling rate, $R(T)$, decreases strongly with temperature. Thus, a negative temperature perturbation leads to more radiation and still lower temperature. Pressure conservation results in a positive density perturbation which also contributes to increased radiation. The density limit experiments on DIII-D have shown that the measured density and temperature for X-point MARFE formation are consistent with the density threshold for the onset of instability.[2] However, a serious weakness lies in the derivation of the empirical scaling which has to resort to the global L-mode transport model with the current scaling. Based on the simulation results in Sec. II B, it is reasonable to believe that increased transport at high densities is responsible for the formation of the X-point MARFE and divertor detachment. The X-point MARFE formation is a natural consequence of the relative competition between parallel heat transport, which scales as $T_e^{7/2}$, and perpendicular turbulence losses, scaling through the impact of collisionality on turbulence level, as an inverse power of the temperature. For pressure conservation, as density increases and temperature decreases, the ratio between parallel and perpendicular power balance scales as T_e^6 and more power flow to the main chamber relative to the divertor plate. Here the estimate is based on the linear scaling of perpendicular turbulence transport with collisionality as inferred from the BOUT runs. The flux tube expansion in passing near the X-point reduces the parallel heat flux there compared to its midplane value upstream. Such a reduction in heat flux leads to a lower temperature and therefore the formation of the density buildup near the X-point due to pressure conservation; reduced T_e can also leads to increased neutral penetration and thus plasma fueling. For a constant impurity fraction (n_I/n_e, n_I is the impurity density), the radiated power $P_{\mathrm{rad}}=n_e n_I R(T)$ increases as the square of the density for a given temperature $[P_{\mathrm{rad}}=n_e^2(n_I/n_e)R(T)]$. Thus, high density regions are capable of large radiation losses, and as the peak in the plasma density shifts to the X-point region, a strong MARFE can form there.

To calculate the MARFE formation and poloidal detachment as a result of the large radial transport, a set of transport equations for particle, momentum, and energy conservation is solved numerically. The different steady-state solutions are obtained using the UEDGE 2D edge transport code[11] by adding strong radial convection while keeping everything else the same. A detailed study of the effect of possible convective transport is reported in Ref. 28. The resulting impurity radiation power contours are shown in Fig. 6 for a constant carbon impurity concentration of 0.5%. In both cases, the

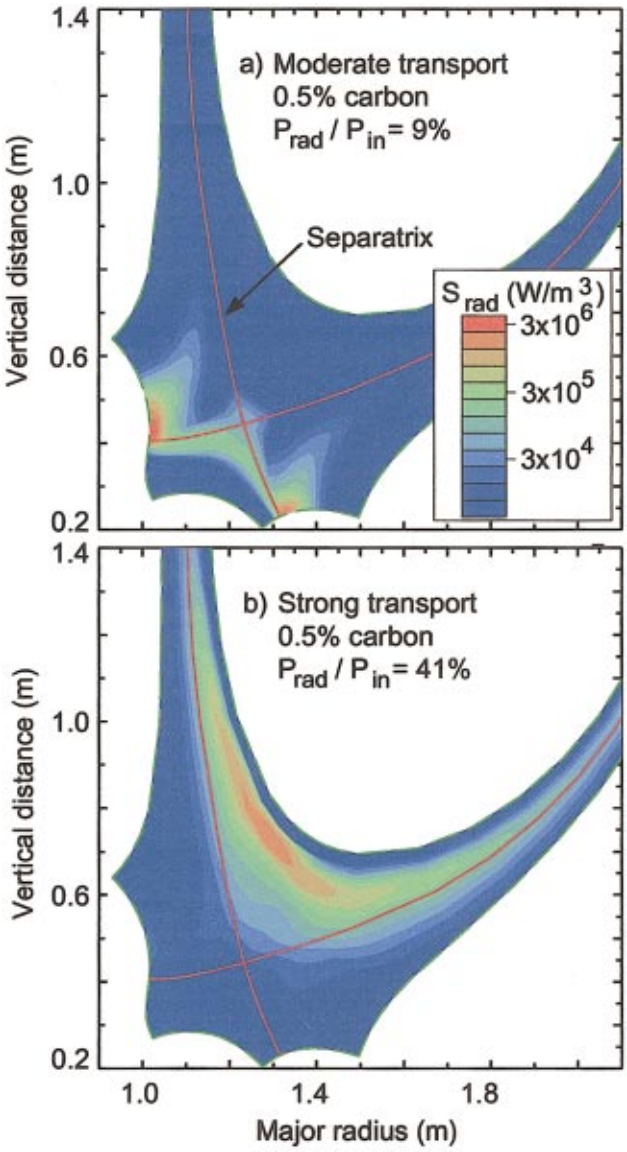

FIG. 6. (Color) The contours of impurity radiation power calculated from UEDGE simulation. (a) The convection velocity v_ψ is zero. (b) The convection velocity v_ψ increases radially from ~40 m/s at the core boundary to 300 m/s at the main chamber wall, extending as a step function from slightly above the X-point to slightly below the top of the machine to emulate the ballooning characteristics found in BOUT simulation.

radial diffusion coefficient for density is 0.5 m^2/s, while for momentum and energy the coefficients are set to 1 m^2/s. The radial convection velocity is everywhere zero for Fig. 6(a), whereas for Fig. 6(b), the convection velocity increases approximately quadratically with radial distance between the core boundary and the wall, being 40 m/s at the core and 300 m/s at the wall. The enhanced convection region is limited to the outer poloidal domain bounded by the top of the machine and a surface 10 cm above the X-point. The *ad hoc* convective velocity is used in UEDGE to emulate the ballooning characteristics found in BOUT simulations discussed above. As the radial transport increases, the peak of cold plasma shifts from the plate to the X-point region, and the MARFE is formed near the X-point. The calculated ratio of the radiated power to input power $P_{\mathrm{rad}}/P_{\mathrm{in}}$ is 9% for normal trans-

port, and 41% for the enhanced transport. It is important to note that the evolution to the MARFE-like state appears sensitive to the level of the enhanced transport near the core boundary; if the enhanced convection is zero on this boundary, while still rising to large values at the wall, the MARFE is not formed. Even though the model is not yet a self-consistent, closely coupled turbulence-transport simulation, the case with enhanced convection at the core boundary does qualitatively support the scenario that the large midplane transport leads to cold plasma shifting to the X-point region. With the associated drop in the separatrix temperature, the hot core plasma is eroded, and the current and pressure profiles should shrink if they were evolved, leading to MHD instability. In order to simulate the real experiment, time-dependent feedback between turbulence and transport processes needs to be included. Since the diffusion coefficient calculated from BOUT is quite high as the density limit is approached or exceeded, it is expected that the turbulence will significantly affect plasma profiles, which in turn change the turbulent transport and MHD modes, and finally the core plasma either reaches some marginal stability point or disrupts.

IV. DENSITY LIMIT SCALING WITH CURRENT

The empirical experimental database shows that the simple global scaling law for the density limit, $n_G = I_p/\pi a^2$, works for a wide variety of machine sizes and configurations, for limited and diverted machines, and for all first wall materials and geometry. The above sections have discussed that plasma boundary turbulence and transport is responsible for edge cooling, MARFE formation, and divertor detachment, which ultimately leads to the density limit. These two observations indicate that plasma current may play a key role in controlling conditions giving rise to enhanced plasma turbulent transport. The dominant current scaling for the turbulence calculation could arise either from the poloidal magnetic field or through the parallel magnetic connection length via the magnetic equilibria.

The current scaling of the density limit has been extrapolated from an additional series of numerical experiments to examine changes in the turbulent transport due to changes in the plasma current. The series of magnetic equilibria have been generated by using the MHD equilibrium package within Corsica,[15] where the experimentally measured plasma pressure profiles are used and kept fixed. It is found that the turbulent transport is consistently reduced due to the associated increase in the equilibrium magnetic field (by fixing q profiles in Corsica) at all density, as shown in Fig. 7. This suggests that the dominant current scaling arises from the toroidal field rather than through a connection length. Because plasma safety factor q is fixed, the increase in plasma current leads to increase of poloidal and toroidal fields, which in turn leads to the decrease of plasma beta and turbulence. Figure 7 also shows that for the fixed density and temperature plasma profiles, as the current decreases, transport increases but exhibits a nearly discontinuous behavior from $I_p = 1.46$ MA to $I_p = 1.22$ MA for $x < 1$ cm. The implication is that a catastrophic boundary is crossed.

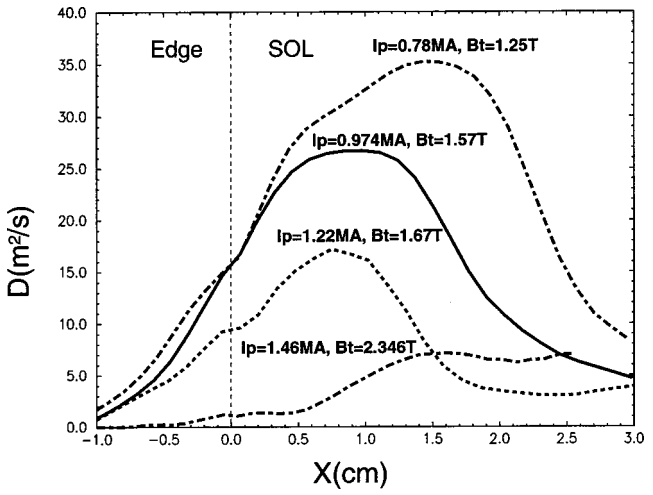

FIG. 7. Profiles of diffusion coefficients versus current calculated from BOUT simulations at high density.

In the above-mentioned density limit experiments on DIII-D, an expression for MARFE stability in terms of global variables has been derived from the local stability equations by using the L-mode scaling law to eliminate temperature and employing a simple fit to the radiation curves.[2,3] This exercise yields the similar empirical expression for n_G, while the applicability of global scaling laws to the plasma boundary and assumptions which relate local to average density are somewhat questionable. Figure 8 is a plot of the maximum of diffusion coefficients from Fig. 7 versus current which indeed shows that local transport scaling with the current is a reminiscence of the global L-mode transport model ($\tau_E \propto I_p$). Thus the match of the empirical scaling is not merely a coincidence!

Figure 9 shows a contour plot of transport coefficient (averaged poloidally and toroidally) at the separatrix versus plasma current and density. We have conducted 17 additional BOUT runs for five different densities and four different cur-

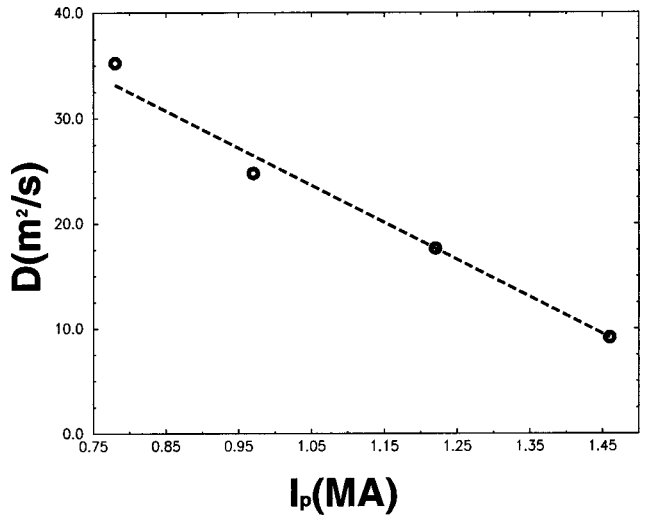

FIG. 8. A plot of the maximum of diffusion coefficients from Fig. 7 versus current which shows that local transport scaling with the current is a reminiscence of the global L-mode transport model ($\tau_E \propto I_p$).

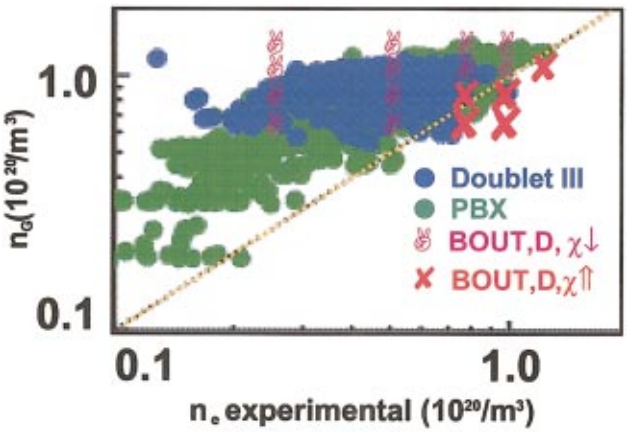

FIG. 9. (Color) A contour plot of transport coefficient at separatrix versus plasma current $n_G = I_p/\pi a^2$ and density. The large transport boundary (at the separatrix $D \geqslant 10\ m^2/s$) shown by the ×'s is consistent with experimental operational limit.

rents. For a given current, as the density approaches or exceeds the Greenwald density, the region of high transport extends inside the last closed flux surface. We choose the effective diffusion coefficient at the separatrix of $D = 10\ m^2/s$ as the boundary for the density limit. This boundary is consistent with the Greenwald density line. Thus it becomes clear that turbulent transport plays a fundamental role in the plot which shows the important relation between the maximum attainable plasma density and the current. The large turbulent transport very likely leads to a collapse of the edge plasma as the density approaches or exceeds the Greenwald density.

The parametric scaling of the density limit in tokamak plasma has been an active research subject since the late 1970s. Here we demonstrate that the turbulent transport is consistently reduced due to increases in the plasma current (by fixing q profiles in Corsica). In order to determine the q scaling, we also conduct a second set of scaling runs by fixing the B_t profile in Corsica. Unfortunately, there is no global trend for changes in transport associated with changes in the parallel connection length $L_\parallel$ ($L_\parallel \sim qR$) over the whole boundary region across the separatrix at high density. In the region near the separatrix, the turbulent transport increases as I_p increases, while in the far SOL, the turbulent transport decreases for the same variation of I_p. The underlying mechanisms are still under investigation. We plan to conduct more BOUT runs to test the q scaling by fixing B_t profiles in Corsica, and alternatively to determine the dependence of the density limit on B_t by fixing I_p in Corsica. Additional dependencies on q may also come from plasma parallel equilibrium physics and/or long wavelength MHD modes that may contribute to the current scaling of the density limit. We therefore defer more complete parametric scaling studies in a future publication.

V. SUMMARY AND DISCUSSIONS

Understanding the density limit is crucial for projecting the performance of future fusion machines. In this article, we have presented a model for density limit in tokamak plasma based on the edge simulation results from BOUT and UEDGE codes. Simulations of turbulence in tokamak boundary plasmas show that turbulent fluctuation levels and transport increase with collisionality. At high density, the perpendicular turbulent transport dominates the parallel classical transport, leading to substantially reduced contact to the divertor and the destruction of the edge E_r shear layer, and the region of high transport extends inside the last closed flux surface. As the density increases, these simulations show resistive X-point mode→resistive ballooning modes →detachment from divertor. The simulations also show that it is easier to reach the density limit as the density increases while holding pressure constant than holding temperature constant. UEDGE 2D transport simulations with increasingly large radial outboard transport, as indicated by BOUT for increasing density, shows that such transport can lead to an X-point MARFE when impurity radiation is included, which is a common symptom of density-limit related disruption. BOUT also demonstrates that the local transport scaling with the current is a reminiscence of the global L-mode transport model ($\tau_E \propto I_p$) (by fixing q profiles). This current scaling appears on a plot of discharge current versus density as an abrupt increase in the radial transport as the Greenwald density is approached or exceeded. All of these results indicate that rapid edge cooling due to large radial transport is a key for the physics of the tokamak density limit.

Even though progress has been made in elucidating several important underlying processes, such as turbulence, transport, impurity radiation, and neutral recycling, the present work is far from complete. The models are simplified and decoupled. There are still important remaining questions to be answered. For example, what is the dependence of density limit on q and B_t? How does the density limit calculated from turbulence and transport codes depend on core power? How can we better parametrize the density limit caused by the rapid edge cooling in terms of pedestal density and temperature, rather than line-averaged density? Since the physics of the density limit is complex and highly nonlinear, and its full evolution involves transport and atomic processes, it is essential that self-consistent models for sources, sinks, turbulence, transport, and MHD are used. Integrating these components is the subject of ongoing research.

ACKNOWLEDGMENTS

We are pleased to acknowledge useful conversations with J. Boedo, K. H. Burrell, R. H. Cohen, P. H. Diamond, D. A. D'Ippolito, R. J. Groebner, S. I. Krasheninnikov, B. LaBombard, R. Moyer, J. R. Myra, G. D. Porter, M. E. Rensink, R. Schneider, M. N. Rosenbluth, D. D. Ryutov, J. Terry, and S. Zweben.

This work was performed under the auspices of the U.S. Department of Energy by the University of California, Lawrence Livermore National Laboratory under Contract No. W-7405-Eng-48, by MIT under Contract No. DE-FC02-99ER54512, and by General Atomics under Contract No. DE-AC03-99ER54463.

[1]M. Greenwald, J. L. Terry, S. M. Wolfe, S. Ejima, M. G. Bell, S. M. Kaye, and G. H. Neilson, Nucl. Fusion **28**, 2199 (1988).
[2]M. A. Mahdavi, R. Maingi, R. J. La Haye *et al.*, in *Proceedings of the 24th European Physical Society Conference on Controlled Fusion and Plasma Physics*, Berchtesgaden, Germany, 9–13 June 1997, edited by M. Schittenhelm, R. Bartiromo, and F. Wagner (European Physical Society, Petit-Lancy, 1997), Vol. 21A (part III) (ECA), p. 1113.
[3]R. Maingi, L. R. Baylor, T. Jernigan *et al.*, in *Proceedings of the 17th International Conference on Fusion Energy*, Yokohama, 1998 (International Atomic Energy Agency, Vienna, 1998), Vol. 2, p. 793.
[4]M. A. Mahdavi, T. H. Osborne, A. W. Leonard *et al.*, Nucl. Fusion **42**, 52 (2002).
[5]M. Greenwald, Plasma Phys. Controlled Fusion **44**, R27 (2002).
[6]F. C. Schuller, Plasma Phys. Controlled Fusion **37**, A135 (1995).
[7]B. Lipschultz, J. Nucl. Mater. **135–147**, 15 (1987).
[8]B. N. Rogers, J. F. Drake, and A. Zeiler, Phys. Rev. Lett. **81**, 4396 (1998).
[9]S. I. Krasheninnikov, Phys. Lett. A **283**, 368 (2001).
[10]X. Q. Xu, R. H. Cohen, T. D. Rognlien, and J. R. Myra, Phys. Plasmas **7**, 1951 (2000).
[11]T. D. Rognlien, D. D. Ryutov, N. Mattor, and G. D. Porter, Phys. Plasmas **6**, 1851 (1999); T. D. Rognlien, B. J. Braams, and D. A. Knoll, Contrib. Plasma Phys. **36**, 105 (1996).
[12]S. I. Braginskii, ''Transport processes in a plasma,'' in *Reviews of Plasma Physics*, edited by M. A. Leontovich (Consultants Bureau, New York, 1965), Vol. I, p. 205.
[13]T. D. Rognlien, X. Q. Xu, and A. C. Hindmarsh, J. Comput. Phys. **175**, 249 (2002).
[14]L. L. Lao, H. St. John, R. D. Stambaugh, A. G. Kellman, and W. Pfeiffer, Nucl. Fusion **25**, 1611 (1985).
[15]L. D. Pearlstein, R. H. Bulmer, T. A. Casper, E. B. Hooper, R. A. Jong, T. B. Kaiser, L. L. LoDestro, and H. L. Berk, in *Proceedings of the 28th European Physical Society Conference on Controlled Fusion and Plasma Physics*, Madeira, Portugal, 18–22 June 2001, edited by C. Silva, C. Varandas, and D. Campbell (European Physical Society, Funchal, 2001), Vol. 25A (ECA), pp. 1901–1904.
[16]X. Q. Xu, W. M. Nevins, R. H. Cohen, J. R. Myra, and P. B. Snyder, New J. Phys. **4**, 53.1 (2002).
[17]X. Q. Xu, R. H. Cohen, W. M. Nevins *et al.*, Nucl. Fusion **42**, 21 (2002).
[18]A. Mazurenko, M. Porkolab, D. Mossessian, J. A. Snipes, X. Q. Xu, and W. M. Nevins, Phys. Rev. Lett. **89**, 225004 (2002).
[19]W. M. Nevins, X. Q. Xu, T. N. Carlstrom *et al.*, in *Proceedings of the 19th International Conference on Fusion Energy*, Lyon, France, 14–19 October 2002 (International Atomic Energy Agency, Vienna), IAEA-CN-94/THP3/07.
[20]P. N. Guzdar, J. F. Drake, D. McCarthy, A. B. Hassam, and C. S. Liu, Phys. Fluids B **3**, 3712 (1993).
[21]X. Q. Xu, R. H. Cohen, G. D. Porter *et al.*, Nucl. Fusion **40**, 731 (2000).
[22]J. R. Myra, D. A. D'Ippolito, X. Q. Xu, and R. H. Cohen, Phys. Plasmas **7**, 2290 (2000).
[23]D. L. Brower, C. X. Yu, R. V. Bravenec *et al.*, Phys. Rev. Lett. **67**, 200 (1991).
[24]B. LaBombard, R. L. Boivin, M. Greenwald, J. Hughes, B. Lipschultz, D. Mossessian, C. S. Pitcher, J. L. Terry, and S. J. Zweben, Phys. Plasmas **8**, 2107 (2001); B. LaBombard, M. Greenwald, R. L. Boivin, B. A. Carreras, J. W. Hughes, B. Lipschultz, D. Mossessian, C. S. Pitcher, J. L. Terry, and S. J. Zweben, ''Density limit and cross-field edge transport scaling in Alcator C-Mod,'' in *Proceedings of the 19th International Conference on Fusion Energy, Lyon, France, 14–19 October 2002* (International Atomic Energy Agency, Vienna), IAEA-CN-94/EX/D2-1.
[25]R. Moyer, J. W. Cuthbertson, T. E. Evans, G. D. Porter, and J. G. Watkins, J. Nucl. Mater. **241–243**, 633 (1997).
[26]M. Endler, Nucl. Fusion **35**, 1307 (1995).
[27]V. A. Vershkov, S. A. Grashin, V. V. Dreval, V. V. Piterskii, S. V. Soldatov, and A. N. Jakovets, J. Nucl. Mater. **241–243**, 873 (1997).
[28]A. Yu. Pigarov, S. I. Krasheninnikov, T. D. Rognlien, M. J. Schaffer, and W. P. West, Phys. Plasmas **9**, 1287 (2002).